Electrical nanopatterning of TiO_2 single crystal surfaces in situ via local resistance and potential switching

C. Rodenbücher, D. Wrana, P. Meuffels, M. Rogala, F. Krok, and K. Szot

Citation: APL Materials **6**, 066105 (2018); doi: 10.1063/1.5028424
View online: https://doi.org/10.1063/1.5028424
View Table of Contents: http://aip.scitation.org/toc/apm/6/6
Published by the American Institute of Physics

APL MATERIALS **6**, 066105 (2018)

Electrical nanopatterning of TiO_2 single crystal surfaces *in situ* via local resistance and potential switching

C. Rodenbücher,[1] D. Wrana,[2] P. Meuffels,[1] M. Rogala,[3]
F. Krok,[2] and K. Szot[1,4]
[1]*Forschungszentrum Jülich GmbH, Peter Grünberg Institute (PGI-7), JARA-FIT, 52425 Jülich, Germany*
[2]*M. Smoluchowski Institute of Physics, Jagiellonian University, 30-348 Krakow, Poland*
[3]*Department of Solid State Physics, University of Lodz, 90-236 Lodz, Poland*
[4]*A. Chełkowski Institute of Physics, University of Silesia, 40-007 Katowice, Poland*

(Received 10 March 2018; accepted 17 May 2018; published online 12 June 2018)

The resistive switching effect in transition metal oxides allows for a dedicated manipulation of the oxide resistance via electrical stimuli. Here, we perform local-conductivity atomic force microscopy simultaneously with the Kelvin probe force microscopy under ultra-high vacuum conditions using the very same tip investigating the very same sample area to monitor the surface conductivity and surface potential of thermally reduced TiO_2 single crystals. We show that the resistance of confined surface areas can be switched by applying a voltage of several volts to the tip during scanning in the contact mode. By conducting *in situ* oxidation experiments, we present that this surface switching is related to a local redox reaction, which can be controlled electrically allowing for surface nanopatterning and illustrates the capability of transition metal oxides for multilevel resistive switching being a prerequisite for neuromorphic computing. We discuss that the features of the electrically engraved nanopattern can be scaled down to a lower boundary at several tens of nanometers. The observed limit around 25 nm is determined by the presence of intrinsic local variations in electrical surface properties appearing as a common phenomenon of slightly reduced metal oxide surfaces. https://doi.org/10.1063/1.5028424

In recent years, transition metal oxides attracted a lot of attention since their surface properties can be modified easily, which can be exploited for various future energy and information technologies ranging from photovoltaics, catalysis, and molecular electronics to memristive data storage and neuromorphic logic applications.[1–6] As a binary dielectric, TiO_2 in rutile structure has become a prototype oxide for investigations of the manipulation of its electronic properties. It has been shown that redox processes can be induced easily by external gradients of the electrical or chemical potential leading to the generation or annihilation of oxygen vacancies which in turn changes the valence state of the Ti ion due to charge compensation effects.[7–9] This way, an insulator-metal transition can be induced upon thermal reduction changing the resistance of the oxide over many orders of magnitude. In extensive studies on resistive switching devices based on transition metal oxides such as TiO_2, it has been elaborated that this valence change mechanism (VCM) is responsible for resistive switching. The underlying mechanism was found to be the movement of active ions (here oxygen) under an electric field, and also electron trapping effects have been discussed to be involved in the switching process.[10,11] Since in the Ti-O system various stable crystallographic phases exist, upon prolonged reduction of a single crystal induced either thermally or electrically under reducing conditions, the oxygen vacancies can eventually agglomerate and create titanium suboxides such as Magnéli phases.[12–14] This effect can have a distinct local nature as was found by electron microscopy on memristive TiO_2 devices, in which switchable nanofilaments consisting of Ti_nO_{2n-1} are created during an initial electroforming step.[15–22] In order to investigate the fundamental nature of the valence

change mechanism, nanoscale investigations using the tip of a local-conductivity atomic force microscope (LC-AFM) as a mobile electrode are the methods of choice. So far, many experiments have been performed on TiO_2 thin films as well as on single crystals revealing the possibility to switch the local conductance state of surface areas in the nanometer range.[16,23–27] Similar results have been obtained on other binary oxides such as NiO.[16,28] It was found that the switched surface shows local variations in surface conductivity which were attributed to the influence of extended defects such as linear arrangements or clustering of oxygen vacancies interacting with dislocations.[26] Combining LC-AFM switching experiments with investigations using a Kelvin probe force microscope (KPFM) in ambient revealed that the change in the conductance is related to a distinct change in surface potential which was attributed to the ex- and incorporation of oxygen during the switching process.[24] Here, we employ the method of surface switching *in situ* under ultra-high vacuum conditions to avoid any external influence on the redox processes. At first, we investigate the slightly reduced TiO_2 (110) surface as an initial state and correlate the variations in local current maps that are typically found on metal oxide surfaces with spatial variations in surface potential. We demonstrate that by addressing the surface, different conductance and potential states can be generated depending on the tip voltage allowing for purely electrical nanopatterning without changing the morphology of the surface. We show that the real scaling limit of nanopatterning determined by the local variations is in the range of a few tens of nanometers. Thanks to the simultaneously derived information about local conductivity and local surface potential, our findings shed light on the electrical nature of the surface and nanoscale resolution limit of potential memristive data storage on transition metal oxide surfaces.

We investigated the epi-polished (110) surface of Verneuil-grown TiO_2 single crystals obtained from Shinkosha. In order to induce a significant amount of oxygen vacancies into the initially insulating crystals, annealing under UHV conditions (maintained by an ion pump) was performed using a ceramic heater. During the annealing at 750 °C for 30 min for LC-AFM investigations, the total pressure stayed below 10^{-7} mbar. The surface temperature was controlled by using a pyrometer. After cooling down to room temperature, the specimen was transferred *in situ* to the measurement chamber of a JEOL JSPM 4610 atomic force microscope operating at a pressure below 4×10^{-10} mbar. LC-AFM measurements were performed using PtIr-coated contact mode tips (Nanosensors PPP-ContPt) being stable in terms of wear, allowing for high lateral resolution, and are widely used as conducting tips in contact mode AFM. In addition, Pt electrodes are often employed in real oxide devices; hence, tips used in presented study can be regarded as mobile nanoelectrodes reflecting the situation of prototypical memristive devices. In order to obtain information about the surface potential difference simultaneously to the local conductivity, the KPFM was performed in the non-contact mode with a single pass technique using the very same tips. To stabilize the cantilever oscillation in vacuum, the 7th harmonics of the fundamental mode was used as a control parameter of the feedback loop, keeping the force between the tip and sample constant during KPFM measurements. This way, the contact potential difference (*CPD*) as the difference of the work function of the surface and the tip (approx. 5.7 eV) is measured. To determine the reduction state of the surface upon thermal annealing, *in situ* X-ray photoelectron spectroscopy (XPS) was performed using a PHI 5700/660 instrument from Physical Electronics, with monochromatized Al-Kα radiation under UHV conditions. For XPS measurements, the samples were annealed stepwise to 600 °C, 700 °C, and 800 °C and subsequently cooled down to 400 °C. During each annealing step which lasted for several hours, the core line spectra of Ti2*p* and C1*s* were recorded at the specific temperature as shown in Fig. 1(a). It can be seen that the Ti2*p* line showing one doublet corresponding to the valence state 4+ accompanied by two shake up peaks at higher binding energy did not change upon the annealing experiment. This confirmed that after thermal reduction at these moderate temperatures the surface is in a slightly reduced state without a significant amount of new phases formed. Regarding the C1*s* line, a distinct peak coming from chemisorbed carbon can be seen at the first temperature step (600 °C) which completely vanished after annealing at 700 °C. Hence we decided to use the TiO_2 surface annealed at 750 °C by LC-AFM and KPFM in order to investigate a slightly reduced but carbon free sample. To analyze the macroscopic electrical transport, we performed conductance measurements during thermal annealing on a ceramic heater under UHV conditions as shown in Fig. 1(b). The temperature was ramped up to 750 °C within a couple of minutes and then held at this

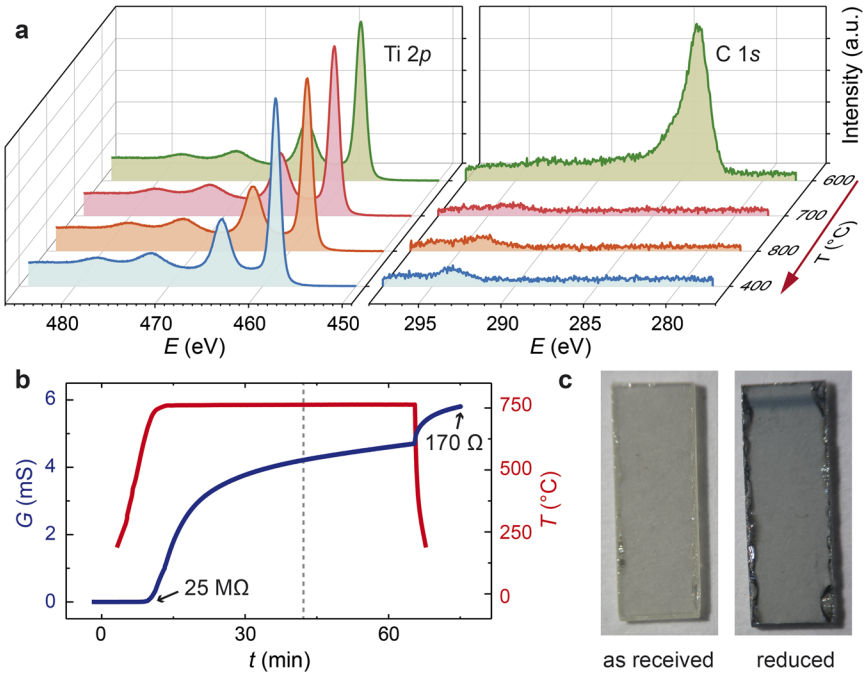

FIG. 1. Thermal reduction of TiO_2. (a) XPS core line spectra (intensity vs. binding energy E) of Ti2p and C1s measured *in situ* at different annealing temperatures under UHV conditions. (b) Conductance of an $8 \times 3 \times 0.5$ mm^3 single crystal during annealing and subsequent cooling under UHV conditions. (The gray dashed line marks the annealing time used for LC-AFM investigations.) (c) Optical micrographs of the crystal before and after reduction.

temperature for 1 h before cooling down rapidly to room temperature as shown as a red curve (due to the measurement by the pyrometer, only values above 200 °C are available). The blue curve displays the conductance measured using the lock-in technique with a voltage of V_{rms} = 10 mV (f = 532 Hz). It can be seen that upon annealing the conductance increases significantly within the first minute of reduction corresponding to a decrease in the resistance by many orders of magnitude. After approximately 30 min of keeping the crystal at 750 °C, the slope of the conductance-time curve had become approximately constant and the curve shows a nearly linear behavior [see the gray dashed line in Fig. 1(b)]. Hence, we chose this time as preparation time for the slightly reduced samples investigated by LC-AFM below. The conductance of the sample kept increasing up to 1 h reduction time, and then the heater was turned off. Upon cooling, the conductance of the sample further increased indicating metallic behavior. Optical inspection of the sample after annealing revealed that the color had changed from almost transparent to a bluish but still significantly translucent color. Together with the analysis of the electronic structure, we can conclude that although the macroscopic electronic transport properties had been modified from highly insulating up to metallic, the sample was still in a slightly reduced state with a Ti valence of 4+ and an only moderate increased optical absorption. This could also serve as an indication that the electronic transport in this stage of reduction is locally confined.[29]

We start with the analysis of the nanoscale electronic properties of the slightly reduced surface (750 °C UHV, 30 min). Using a read voltage of 0.1 V, we recorded a LC-AFM current map of a region of 1 μm^2 presented in Fig. 2(a). By operating the contact-mode cantilever in the non-contact mode, we were able to obtain also a *CPD* map of the very same region [Fig. 2(b)]. It can be seen that in both maps local variations in the electronic properties are present showing a grainy, cloud-like structure with typical dimensions in the range of 10-40 nm. In order to visualize these variations, histograms of the conductance and the *CPD* were calculated [Figs. 2(c) and 2(d)]. The conductance histogram can be simulated by a log-normal distribution [red curve in Fig. 2(c)] reflecting its inhomogeneous nature, while the *CPD* histogram is close to a normal distribution [red curve in Fig. 2(d)]. To illustrate the impact of the spatial variations on the electrical characteristics,

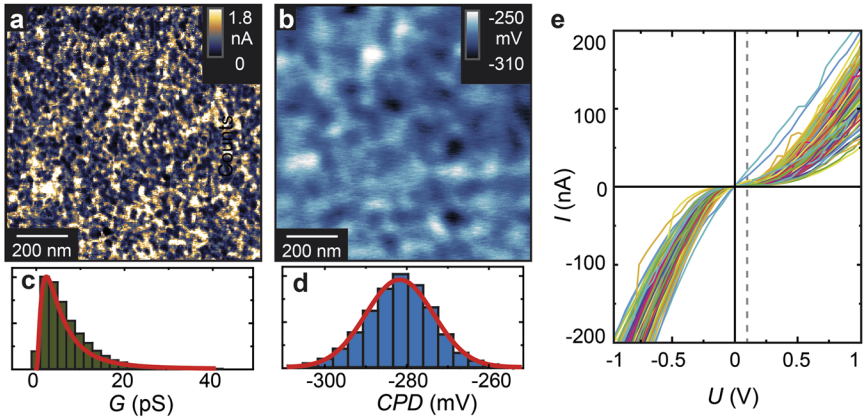

FIG. 2. Electrical properties of the slightly reduced TiO_2 (110) surface. (a) LC-AFM current map measured with a tip voltage of 0.1 V. (b) KPFM surface potential measurement of the very same region. Histograms of conductance (c) and contact potential difference (d) extracted from the maps (a) and (b), respectively. (e) IV characteristics collected by sweeping the tip voltage at 100 different randomly selected points of the surface. The dotted line marks the LC-AFM read voltage used in (a).

IV curves were obtained at 100 randomly selected points of the surface by sweeping the voltage applied via the AFM tip between −1 V and +1 V as shown in Fig. 2(e). The apparent highly nonlinear relation between current and voltage reflects the electronic transport of the tip-surface system. In agreement with the LC-AFM maps, a distinct variation in the IV curves is present as a result of local inhomogeneities.

To understand the differences in the local variations in local conductivity and surface potential, basic properties of a tip-surface system should be discussed. In general, between a metal and a semiconductor, an energy barrier (Schottky barrier) is formed[30,31] depending on the work function differences of the materials. The height of this barrier can also be modulated by interface states leading to a pinning of the Fermi energy (Bardeen barrier).[32] Additionally, contaminations or adsorbate layers could contribute to the energy barrier between the metal and semiconductor, in particular, in a LC-AFM experiment with the tip as the mobile electrode. Regarding Fig. 2, it can be clearly seen that the relation between current and voltage is not a pure Schottky curve. On the other hand, the curves are also not completely linear as would be expected for an Ohmic contact in the absence of an energy barrier. Hence we can assume that the current between the tip and sample can be related to processes such as tunneling through the barrier or thermionic emission leading to a non-linear dependence of the current on the barrier height. Following this consideration, the differences in variations in current and *CPD* maps can be understood. Since the normal-distributed variations in *CPD* can be regarded as a measure for variations in surface barrier height, they will be amplified to a lognormal distribution in current due to the non-linear relation. This effect was also observed by LC-AFM investigations on the second prototypical metal oxide $SrTiO_3$ indicating that local variations in electronic properties on the nanoscale are a common effect on slightly reduced metal oxide surfaces.[33]

As the origin of the variations in local barrier height and conductivity, we can suspect that the oxygen vacancies induced upon thermal reduction are not homogeneously distributed in the surface layer. Generally, in TiO_2, a rearrangement or clustering of vacancies in the surface layer can be induced easily[3] and can be additionally influenced by the presence of extended defects such as dislocations, which are introduced with high density close to the surface due to the mechanical polishing of the single crystals done by the manufacturer. Since the crystals were annealed and measured under UHV conditions, contamination by impurities such as carbon can be excluded as confirmed by XPS (Fig. 1). In order to investigate the direct impact of redox processes on the electrical surfaces, we performed *in situ* oxidation experiments by dosing a small amount of oxygen (440 L) with a pressure of 5×10^{-7} mbar inside the UHV chamber. Simultaneously, we recorded the average *CPD* value evolution by KPFM line scanning shown in Fig. 3(a) as a function of the oxidation time. Here, changes in *CPD* can be attributed to changes in surface potential only since a tip consists of inert Pt/Ir and does

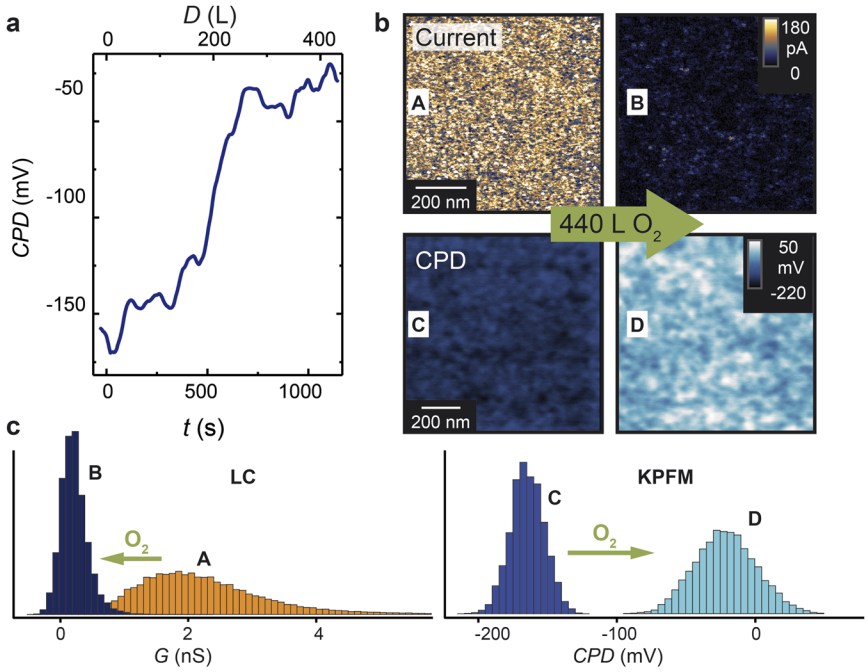

FIG. 3. *In situ* re-oxidation of the slightly reduced TiO_2 (110) surface. (a) Evolution of the average *CPD* value upon oxidation under 5×10^{-7} mbar O_2 obtained by KPFM line scanning. (b) Current (U = 10 mV) and *CPD* maps ($1 \times 1\ \mu m^2$) obtained before (left) and after (right) oxidation. (c) Corresponding histograms of conductance (left) and *CPD* (right).

not change upon oxygen exposure.[34] It can be seen that during the first 500 s of oxygen exposure, the *CPD* increases by more than 100 mV. The comparison of current and *CPD* maps obtained before and after oxidation [Fig. 3(b)] reveals that with the increase in *CPD*, the surface conductivity is decreased and the majority of the measured surface has become insulating with a current below the detection limit of LC-AFM. Only a few conducting spots can still be observed, indicating that some current paths, presumably supported by extended defects,[26] are more resistant toward oxidation than others. This is further illustrated by the histograms [Fig. 3(c)] calculated from the maps of current and *CPD*. Before oxidation, the conductance histogram shows a broad distribution with characteristic lognormal distribution (A). After oxidation, the distribution is significantly narrowed with most of the values being close to the noise level (B). The *CPD* with its initial normal distribution (C) gets shifted to higher values and additionally gets broadened upon oxidation indicating that the inhomogeneity of the surface is increased. This supports the assumption that not all areas of the surface react identical upon oxidation but that the oxygen vacancies close to extended defects such as dislocations are more stable with respect to reoxidation than single surface or subsurface vacancies in agreement with the finding obtained on the heavier reduced TiO_2 surface.[26]

Having proven that the slightly reduced TiO_2 surface is very sensitive to redox processes, we now exploit this effect for electrical nanopatterning as an illustration of the resistive switching capability. Here, we turn back to the freshly reduced surface and scan in the contact mode with a higher writing voltage applied. To maintain the stability of the feedback loop controlling the force between the tip and sample, the scan rates for writing were relatively low resulting in an application time of the writing voltage up to several microseconds per pixel. As shown in the grayscale inset of Fig. 4(a), a pattern consisting of 12 squares having sizes of $200 \times 200\ nm^2$ was written while a different tip voltage between −6 V and +6 V was applied to each square. After this, the conductivity of the modified surface was analyzed by a reading scan with 10 mV bias [Fig. 4(b)]. It can be seen that upon writing with a positive tip voltage, the surface conductivity was increased by more than three orders of magnitude while writing with negative voltage resulted in a significant decrease in conductivity. The *CPD* measurements obtained from the very same modified area may offer an explanation for this behavior [Fig. 4(c)]. Here, a writing with positive bias resulted in a decrease in *CPD* and vice versa as illustrated

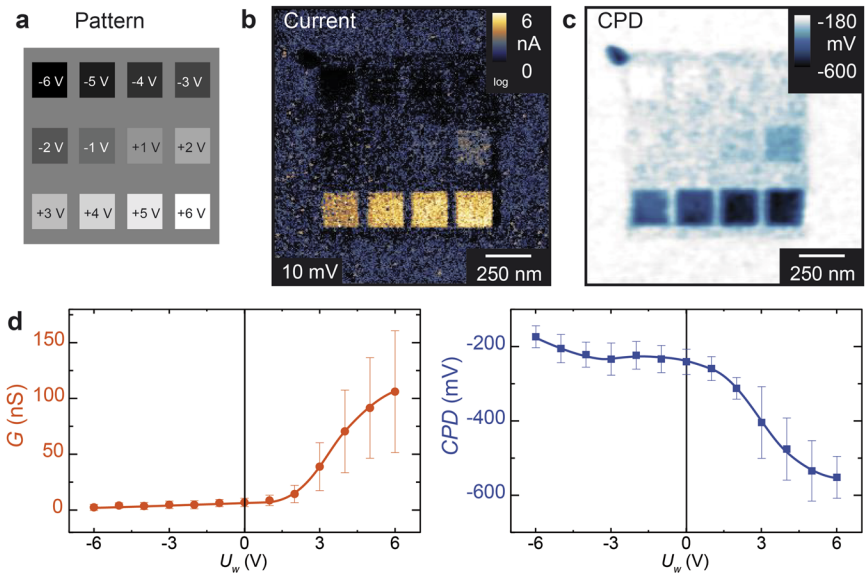

FIG. 4. Electrical tip-induced nanopatterning of the slightly reduced TiO_2 surface. A pattern of squares with different voltages between −6 and +6 V (a) was written and subsequently read by scanning with 10 mV bias (b). (c) Corresponding *CPD* map. (d) Dependence of average conductance and *CPD* value on the writing voltage.

in the plot of the average conductance and *CPD* values in Fig. 4(d) calculated from the maps. This shows that by tuning the writing voltage different resistance states can be induced which illustrates the property of TiO_2 to allow for multilevel resistive switching being a prerequisite for neuromorphic applications. As a side effect, which is often observed in contact mode AFM studies, also the area around the switched squares had slightly lower values of *CPD* and current although here the scanning was performed without bias applied and thus can be attributed to mechanically induced modifications on the sub-nanoscale such as a diffusion or rearrangement of defects in the very near surface region. A further artifact is the non-conducting spot with a low *CPD* value at the upper left corner of the writing area. Before the scan is started, the sample is approached by the tip held at this position and hence there could be a deposition of insulating adsorbates with different work functions from the tip to the surface upon first contact. Considering the relation between oxidation and *CPD* extracted from Fig. 3, we can conclude that the application of a positive voltage leads to a reduction while a negative voltage resulted in an oxidation which could be related to the ex- and incorporation of oxygen from and into the surface layer corresponding to the model presented by Du *et al.*[24] being consistent with models proposed for the eightwise resistive switching in prototypical memristive devices.[35] However, our switching experiments were performed under UHV conditions with much less oxygen available than under ambient conditions, which raises the question that where the oxygen needed for electrical-assisted re-oxidation comes from. Hence, either the oxygen in the vacuum chamber (having an oxygen partial pressure in the range of 10^{-12} mbar) and other oxygen containing gases[36] such as CO_2 could serve as the oxygen source or more complex local redox mechanisms involving a shuffling of oxygen between substoichiometric TiO_x nanophases[3] have to be taken into account. In order to illustrate that the electrical nanopatterning can also be reversible, we at first switched a $(500\ nm)^2$ area to a highly conducting state by scanning with +4 V applied. Subsequently, we performed a further scan with −4 V applied in a $(250\ nm)^2$ area in the center of the previous scan. In the following readout scan performed at 100 mV [Fig. 5(a)], it can be seen that the center area had switched back to low conductivity showing that the tip-induced redox processes allow for write-erase conductivity modifications. Such behavior of switching to ON and OFF states as different polarities is referred to as bipolar resistive switching. Based on the simultaneously measured topography map [Fig. 5(b)], it can be concluded that no significant changes in morphology had occurred during writing and erasing and therefore the surface stayed atomically flat with a *RMS* roughness value of 2.8 Å. The retention of the written state appears to be relatively high under UHV conditions, and sometimes even

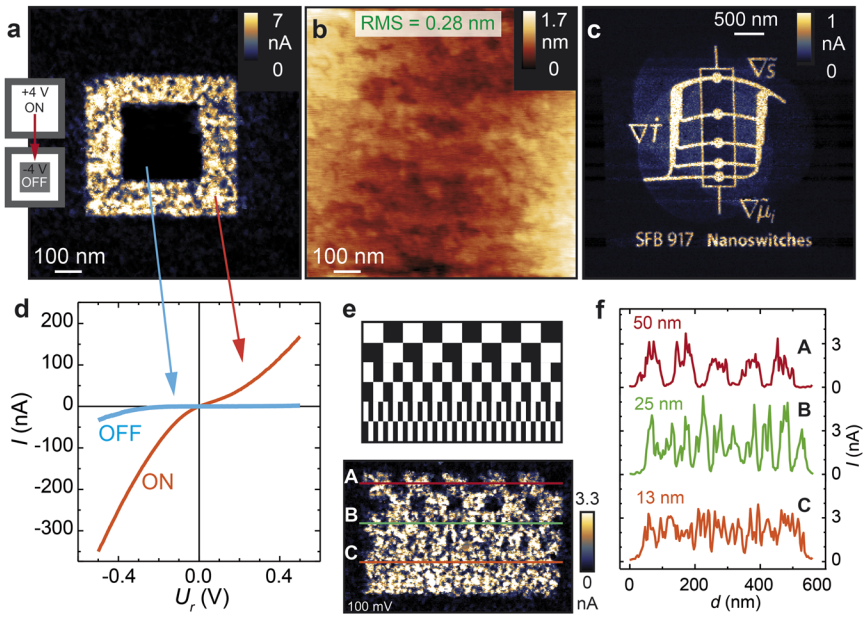

FIG. 5. Erasing and scaling of electrical nanopatterning. (a) Current map (100 mV) after writing a 500 × 500 nm^2 ON pattern with +4 V and subsequently a 250 × 250 nm^2 OFF pattern with −4 V. (b) Corresponding topography map. (c) Current map (10 mV) after writing the SFB 917 logo. (d) IV curves measured in the ON and OFF areas of (a). (e) Current map (bottom) of a region where a nanopattern (top) had been written with +4 V (white rectangles). The line profiles (f) were extracted from regions with three different feature sizes of the nanopattern.

after several tens of hours, we were able to identify the switched region when performing a reading scan. Even when the switched surface was exposed to oxygen, the written pattern remained detectable (see the supplementary material). Finally, as a diverting artwork [Fig. 5(c)], we wrote the logo of our funder, the collaborative research center SFB 917, using a maximum write voltage of +5 V and a readout voltage of 10 mV nicely illustrating the opportunities of electrical nanopattering. Figure 5(d) shows two representative IV curves obtained in the ON and OFF areas of Fig. 5(a), respectively. It can be seen that even at low reading voltages, the current in the ON region is significantly higher than in the OFF region. Additionally, the Schottky-like asymmetry of the OFF curve is less pronounced in the ON curve revealing a more "Ohmic" tendency.

For many technical applications, the scaling limits of oxide devices, e.g., for data storage, are of enormous importance. To investigate to what extent the local variations revealed by the LC-AFM maps of the slightly reduced single crystal surface (Fig. 2) are relevant for scaling, a further nanopatterning experiment was conducted. A binary checkerboard-like pattern with decreasing feature sizes as depicted in the top of Fig. 5(e) was written where white corresponds to a switching voltage of +4 V and black to zero bias. Speaking in terms of digital information storage by resistive switching, black areas could be understood as memory cells storing logical "1" (ON) and white as logical "0" (OFF). The rectangle sizes in the first two columns were 50 nm; in the second two columns, the width of each individual rectangle was limited to 25 nm and in the final column to 13 nm. Readout was performed at 100 mV resulting in the current map shown in the bottom of Fig. 5(e). Apparently, the written information can be directly recognized as a pattern consisting of highly conducting regions representing the ON state separated by the non-written areas representing the OFF state. To address the scaling issue, line profiles with a thickness of 20 nm were extracted from the current map in the three regions of the pattern with different densities plotted in Fig. 5(f). For the 50 nm pattern, the differences between the written and pristine surfaces can unambiguously be distinguished. This also holds partially true for the 25 nm pattern, but a clear assignment of the two conductance states gets difficult since the current values for the ON and OFF regions vary and overlap. For the 13 nm pattern finally, a data readout would be almost impossible since the line profile does not show two distinguishable levels anymore. In particular, the current of the nominally

OFF state rectangles is significantly increased while for the larger rectangles its value was close to the pristine conductivity. This indicates that during writing not only the area directly below the tip has switched but also adjacent parts of the surface got electroreduced to the ON state. Since the contact area between the tip and sample is in the range of a few nm^2 or even less,[37] and it has been already demonstrated that in $SrTiO_3$ single dislocations can be switched, we assume that the broadening of the switching area on the slightly reduced TiO_2 surface is not mainly induced by the tip geometry but is most probably related to surface inhomogeneities such as clustered vacancies having dimensions around 10-20 nm being intrinsically present on the slightly reduced oxide surface (cf. Fig. 2).

In conclusion, we have shown the possibility of performing LC-AFM and KPFM measurements simultaneously under UHV conditions. This way, we were able to prove that on the slightly reduced TiO_2 surface local variations in surface conductivity and surface potential on the nanoscale are present. We investigated the impact of *in situ* redox processes on the nanoscale, showing that re-oxidation of the slightly reduced surface is related to a decrease in conductivity and an increase in surface potential. The possibility of tip-induced memristive switching on the nanoscale was presented. We have demonstrated that by applying writing voltages of several volts to the AFM tip during scanning, it is possible to induce reversible reduction and oxidation processes electrically. Depending on the voltage polarity, surface conductivity and surface potential can be modified allowing for resistive nanopatterning without changing the morphology. By tuning the voltage, different non-volatile resistance states can be written reflecting the multilevel resistive switching properties of TiO_2, which are also a prerequisite for neuromorphic applications. On the length scale of a few tens of nanometers, clearly confined patterns can be written (with an estimated lower limit of approximately 25 nm) demonstrating the ability for memristive data storage. However, a further downscaling of the nanopatterns below 20 nm feature size results in an overlap of switched and non-switched areas, which would lead to a readout error in terms of data storage. This effect appears to be intrinsic and related to slight reduction-induced local variations in the chemical composition of the surface and has to be kept in mind when employing reduced transition metal oxide single crystal surfaces for nanotechnological applications.

See supplementary material for detailed analysis of the stability of the electrically written nanopattern upon oxygen exposure.

We thank J. Friedrich and S. Masberg for technical assistance. M.R. acknowledges the National Science Centre, Poland, Grant No. 2016/21/D/ST3/00955, and D.W. Grant No. 2017/24/T/ST5/00427. This work was supported in part by the Deutsche Forschungsgemeinschaft under Project No. SFB 917 "Nanoswitches."

[1] J. W. Lee, T. Y. Lee, P. J. Yoo, M. Graetzel, S. Mhaisalkar, and N. G. Park, J. Mater. Chem. A **2**, 9251 (2014).
[2] Z. Dohnalek, I. Lyubinetsky, and R. Rousseau, Prog. Surf. Sci. **85**, 161 (2010).
[3] K. Szot, M. Rogala, W. Speier, Z. Klusek, A. Besmehn, and R. Waser, Nanotechnology **22**, 254001 (2011).
[4] D. Wrana, M. Kratzer, K. Szajna, M. Nikiel, B. R. Jany, M. Korzekwa, C. Teichert, and F. Krok, J. Phys. Chem. C **119**, 17004 (2015).
[5] M. Prezioso, F. Merrikh Bayat, B. Hoskins, K. Likharev, and D. Strukov, Sci. Rep. **6**, 21331 (2016).
[6] R. Waser, R. Dittmann, G. Staikov, and K. Szot, Adv. Mater. **21**, 2632 (2009).
[7] X. Pan, M. Q. Yang, X. Fu, N. Zhang, and Y. J. Xu, Nanoscale **5**, 3601 (2013).
[8] M. Rogala, Z. Klusek, C. Rodenbücher, R. Waser, and K. Szot, Appl. Phys. Lett. **102**, 131604 (2013).
[9] K. Szot, G. Bihlmayer, and W. Speier, Solid State Phys. **65**, 353 (2014).
[10] E. Lim and R. Ismail, Electronics **4**, 586 (2015).
[11] C. Kügeler, R. Rosezin, E. Linn, R. Bruchhaus, and R. Waser, Appl. Phys. A **102**, 791 (2011).
[12] P. Waldner and G. Eriksson, Calphad **23**, 189 (1999).
[13] W. Heckel, M. Wehlau, S. B. Maisel, T. Frauenheim, J. M. Knaup, and S. Mueller, Phys. Rev. B **92**, 214104 (2015).
[14] S. G. Park, B. Magyari-Koepe, and Y. Nishi, IEEE Electron Device Lett. **32**, 197 (2011).
[15] J. J. Yang, M. D. Pickett, X. Li, D. A. A. Ohlberg, D. R. Stewart, and R. S. Williams, Nat. Nanotechnol. **3**, 429 (2008).
[16] M. H. Lee, K. M. Kim, S. J. Song, S. H. Rha, J. Y. Seok, J. S. Jung, G. H. Kim, J. H. Yoon, and C. S. Hwang, Appl. Phys. A **102**, 827 (2011).
[17] R. Muenstermann, J. J. Yang, J. P. Strachan, G. Medeiros-Ribeiro, R. Dittmann, and R. Waser, Phys. Status Solidi RRL **4**, 16 (2010).
[18] D.-H. Kwon, K. M. Kim, J. H. Jang, J. M. Jeon, M. H. Lee, G. H. Kim, X.-S. Li, G.-S. Park, B. Lee, S. Han, M. Kim, and C. S. Hwang, Nat. Nanotechnol. **5**, 148 (2010).
[19] C. Nauenheim, C. Kuegeler, A. Ruediger, and R. Waser, Appl. Phys. Lett. **96**, 122902 (2010).

[20] D. Carta, A. P. Hitchcock, P. Guttmann, A. Regoutz, A. Khiat, A. Serb, I. Gupta, and T. Prodromakis, Sci. Rep. **6**, 21525 (2016).
[21] N. Ghenzi, M. J. Sanchez, D. Rubi, M. J. Rozenberg, C. Urdaniz, M. Weissman, and P. Levy, Appl. Phys. Lett. **104**, 183505 (2014).
[22] J. P. Strachan, M. D. Pickett, J. J. Yang, S. Aloni, A. L. D. Kilcoyne, G. Medeiros-Ribeiro, and R. S. Williams, Adv. Mater. **22**, 3573 (2010).
[23] B. J. Choi, D. S. Jeong, S. K. Kim, C. Rohde, S. Choi, J. H. Oh, H. J. Kim, C. S. Hwang, K. Szot, R. Waser, B. Reichenberg, and S. Tiedke, J. Appl. Phys. **98**, 033715 (2005).
[24] Y. Du, A. Kumar, H. Pan, K. Zeng, S. Wang, P. Yang, and A. T. S. Wee, AIP Adv. **3**, 082107 (2013).
[25] P. Bousoulas, J. Giannopoulos, K. Giannakopoulos, P. Dimitrakis, and D. Tsoukalas, Appl. Surf. Sci. **332**, 55 (2015).
[26] M. Rogala, G. Bihlmayer, W. Speier, Z. Klusek, C. Rodenbücher, and K. Szot, Adv. Funct. Mater. **25**, 6382 (2015).
[27] W. Lu, L. M. Wong, S. Wang, and K. Zeng, Phys. Chem. Chem. Phys. **19**, 31399 (2017).
[28] M. Lee, S. Song, K. Kim, G. Kim, J. Seok, J. Yoon, and C. Hwang, Appl. Phys. Lett. **97**, 062909 (2010).
[29] K. Szot and C. Rodenbücher, in *2015 Joint IEEE International Symposium on the Applications of Ferroelectric, International Symposium on Integrated Functionalities and Piezoelectric Force Microscopy Workshop (ISAF/ISIF/PFM)* (IEEE, 2015), p. 143.
[30] E. H. Rhoderick, *Metal-Semiconductor Contacts* (Claredon Press, 1980).
[31] S. M. Sze, *Physics of Semiconductors Devices* (John Wiley & Sons, New York, 1981).
[32] J. Bardeen, Phys. Rev. **71**, 717 (1947).
[33] D. Schaadt, E. Yu, V. Vaithyanathan, and D. Schlom, J. Vac. Sci. Technol., B: Microelectron. Nanometer Struct.–Process., Meas., Phenom. **22**, 2030 (2004).
[34] D. Wrana, C. Rodenbücher, W. Belza, K. Szot, and F. Krok, Appl. Surf. Sci. **432A**, 46 (2018).
[35] D. Cooper, C. Baeumer, N. Bernier, A. Marchewka, C. La Torre, R. E. Dunin-Borkowski, S. Menzel, R. Waser, and R. Dittmann, Adv. Mater. **29**, 1700212 (2017).
[36] K. Szot, J. Keppels, W. Speier, K. Besocke, M. Teske, and W. Eberhardt, Surf. Sci. **280**, 179 (1993).
[37] U. Celano, T. Hantschel, G. Giammaria, R. C. Chintala, T. Conard, H. Bender, and W. Vandervorst, J. Appl. Phys. **117**, 214305 (2015).